Available online at www.sciencedirect.com
ScienceDirect
Journal of Colloid and Interface Science 304 (2006) 323–328
JOURNAL OF Colloid and Interface Science
www.elsevier.com/locate/jcis

Decoration carbon nanotubes with Pd and Ru nanocrystals via an inorganic reaction route in supercritical carbon dioxide–methanol solution

Zhenyu Sun, Zhimin Liu *, Buxing Han, Shiding Miao, Zhenjiang Miao, Guimin An

Center for Molecular Sciences, Institute of Chemistry, Chinese Academy of Sciences, Beijing 100080, China

Received 7 March 2006; accepted 14 September 2006

Available online 19 September 2006

Abstract

This work describes a method to decorate carbon nanotubes (CNTs) with metallic Pd and Ru nanocrystals via inorganic reactions in supercritical (SC) CO_2–methanol solutions. In this route, $PdCl_2$ or $RuCl_3 \cdot 3H_2O$ dissolved in SC CO_2–methanol solution acted as a metal precursor and CNTs functioned as a template to direct the deposition of produced nanoparticles. Methanol served as the reductant for the precursors as well as cosolvent to enhance the dissolution of precursors in SC CO_2. Dry products were readily obtained through in situ extraction with SC CO_2 after reactions. The products were characterized by X-ray diffraction, X-ray photoelectron spectroscopy, and transmission electron microscopy. It was demonstrated that the loading content and particle size of the nanoparticles deposited on CNTs could be tuned by changing the weight ratio of the precursor to CNTs. This simple and efficient approach may also be utilized to synthesize other high-purity materials using inorganic salt precursors in SC CO_2-based solution.

Keywords: Carbon nanotubes; Supercritical fluid; Catalysis; Palladium; Ruthenium; Nanocomposites

1. Introduction

Carbon nanotubes (CNTs) are of scientific interest in nanotechnology and nanodevices because of their superior structural, mechanical, chemical, thermal, and electrical performance [1–4]. Surface modification of CNTs with desired organic, inorganic compounds through covalent and/or noncovalent bonds represents an emerging area in the research on nanotube-based materials. Such modification can result in a significant enhancement of properties and open up a broad range of novel application perspectives. Covalent modification of CNTs has been accomplished mainly by three such approaches as thermally activated chemistry, electrochemical modification, and photochemical functionalization [5]. Noncovalent approaches utilize π-stacking or van der Waals interactions between functional species and CNTs [6]. Recently, noncovalent functionaliztion of CNTs has attracted considerable attention because it is expected to tailor their surface properties, whereby new functions can be implemented while still preserving nearly all the nanotube's intrinsic properties.

Recent advances in attachment of metal nanoparticles to CNTs provide a way to obtain novel hybrid materials with useful properties for gas sensor and catalytic application. For example, single-walled carbon nanotubes (SWNTs) coated with palladium nanoparticles exhibit excellent sensitivity to molecular hydrogen [7]. Multi-walled carbon nanotubes (MWNTs) decorated with gold was proposed as a good candidate material for glucose biosensors [8]. The morphology and size of CNTs make them a suitable catalyst support where catalytically active metal or metallic compound nanoparticles may be immobilized on the surfaces of CNTs. It has been reported that Pt, Ru, and Pt/Ru supported on CNTs show excellent catalytic activities for methanol oxidation in fuel cells as well as for hydrogenation reactions [9–13]. The CNT-supported Rh nanoparticles are very active for hydrogenation of arenes, and the CNT-supported bimetallic Pd/Rh nanoparticles demonstrate extremely high catalytic activity for hydrogenation of anthracene [14]. However, the inert nature of the CNT surface makes it a difficult substrate to attach metal deposits. Despite the impressive results of previous strategies, it remains a challenge to develop simpler and

* Corresponding author.
E-mail address: liuzm@iccas.ac.cn (Z. Liu).

0021-9797/$ – see front matter
doi:10.1016/j.jcis.2006.09.029

more efficient approaches to immobilize metal or metal compounds on CNTs or encapsulate them into the cavities of CNTs.

In recent years, supercritical fluids (SCFs) have been widely utilized in material science because of such properties as low viscosity, high diffusivity, near zero surface tension, and strong solvent power for some small molecules [15–20]. The flexibility of SCFs, in terms of tunable solvation strength and access to high operating temperatures and pressures, enables the synthesis of a variety of nanostructured metal and semiconductor materials. The enhanced wettability and controlled solvation strength readily promote a high uniformity and conformal coverage of complex surfaces and poorly wettable substrates. Among SCFs, supercritical carbon dioxide (SC CO_2) is particularly popular because of its nontoxic and nonflammable nature as well as high density at moderate condition besides the general properties listed above. Therefore, SC CO_2 has been employed as an excellent medium for some chemical processes, including organic reactions [21–23], and separations [15,24,25], etc.

It is known that inorganic salts are generally not soluble in SC CO_2 because CO_2 is nonpolar. However, some polar solvents (e.g., methanol, ethanol, acetone) can act as cosolvents to enhance the solvation power of SC CO_2 significantly [26], which can provide an opportunity for conducting inorganic reactions in SC CO_2-based supercritical solutions. In this work, we developed a one-step route to attach metal (Pd, Ru) nanoparticles to the surfaces of CNTs through inorganic reactions in SC CO_2–methanol solution using $PdCl_2$ and $RuCl_3{\cdot}3H_2O$ as a metal precursor, respectively. Methanol acts as reactant as well as cosolvent to enhance the solubilization of inorganic precursors in supercritical solutions. After reactions, dry and high-purity products are easily obtained by in situ extraction using SC CO_2 as the solvent.

2. Experimental

2.1. Materials

All the chemicals used in this work were of analytical grade, which were commercially obtained and used as received. High-purity (95%) multi-walled CNTs used in this work were provided by Shenzhen Nanotech Port Co., Ltd, which were prepared by the catalytic decomposition of CH_4 using La_2NiO_4 as catalyst precursor. To remove the catalyst, CNTs were purified via being dispersed in a 1 M HNO_3 solution for more than 6 h, followed by filtering and washing with distilled water several times [27]. IR analysis for the treated CNTs showed that no detectable peak was assigned to –COOH group, suggesting the pre-treatment with nitric acid had little influence on the structure of CNTs. The CNTs were characterized with open ends, and their outer diameters and lengths were 40–60 nm and 1–12 μm, respectively.

2.2. Synthesis of Pd–CNT nanocomposites

In a typical experiment, a suitable amount of CNTs dispersed in 5 ml of $PdCl_2$ methanol solution with a concentration of 0.5 mg/ml was loaded into a high-pressure vessel of 22 ml. The vessel was then placed in a constant water bath of 35 °C, and charged with CO_2 up to 9.0 MPa. Subsequently, it was moved to an oven and maintained at 80 °C for about 24 h to ensure the complete conversion of the precursor. The vessel was cooled to 35 °C, and the residual methanol and byproducts in the vessel were extracted with CO_2 at this temperature and 9.0 MPa. After depression, dry products were obtained. By changing the mass ratio of $PdCl_2$/CNTs, products with different Pd contents were achieved.

2.3. Synthesis of Ru–CNT nanocomposites

The procedures to prepare Ru–CNT nanocomposites were similar to those for synthesizing Pd–CNT nanocomposites. In the experiment, some amount of CNTs dispersed in 5 ml of $RuCl_3{\cdot}3H_2O$ methanol solution with a concentration of 0.8 mg/ml was added into a high-pressure reactor of 22 ml. The reactor was placed in a constant water bath of 35 °C, followed by being charged with CO_2 up to 5.0 MPa. It was then moved to an oven of 200 °C and maintained at this temperature for about 5 h. After being cooled to 35 °C, the liquid chemicals in the vessel were extracted with CO_2 at 35 °C and 9.0 MPa and dry products were left in the reactor. By controlling the mass ratio of $RuCl_3{\cdot}3H_2O$/CNTs, products with diverse Ru contents were yielded.

2.4. Characterization

The as-prepared products were characterized by powder X-ray diffraction (XRD) on a D/MAX-RC diffractometer operated at 30 kV and 100 mA with Cu$K\alpha$ radiation. The morphologies and microstructures of the products were examined by means of transmission electron microscopy (TEM) on JEOL JEM-2010 equipped with an energy dispersive X-ray spectrometer with 200 kV operating voltage. X-ray photoelectron spectroscopy (XPS) was performed on an ESCALab220i-XL spectrometer operated at 15 kV and 20 mA at a pressure of about 3×10^{-9} mbar using Al$K\alpha$ as the exciting source ($h\nu =$ 1486.6 eV).

3. Results and discussion

3.1. Synthesis of Pd–CNT nanocomposites

The Pd decorated CNT composites were prepared using $PdCl_2$ as precursor in SC CO_2–methanol solution at 80 °C.

The XRD patterns of pristine CNTs and the as-synthesized products are demonstrated in Fig. 1. It is clear that pattern (a) shows the characteristic diffraction peaks at 26.5°, 43.2°, 44.6°, 54.2°, and 77.7°, which correspond to (002), (100), (101), (004), and (110) reflections of graphite, respectively [28]. Besides those peaks of graphite, the typical diffraction peaks exhibited in pattern (b) at 40.1°, 46.7°, and 68.7° can be well indexed as reflections of crystalline Pd(0) [29]. The XRD results indicate that metallic Pd was produced in the reaction process. A relatively minor diffraction peak appearing at 35.4° is related

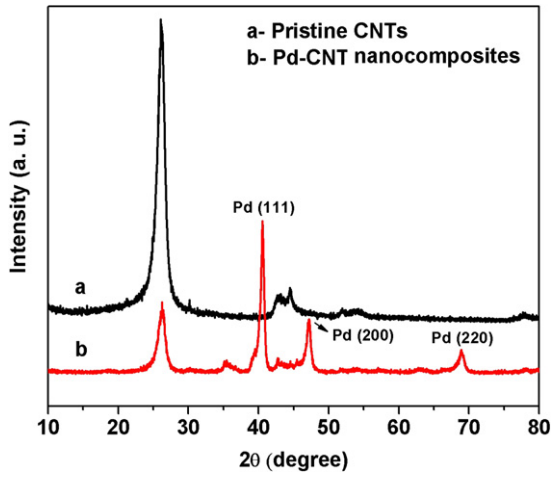

Fig. 1. XRD patterns of (a) pristine CNTs, (b) Pd–CNT composites prepared with the initial $PdCl_2$/CNTs weight ratio of 1:1.

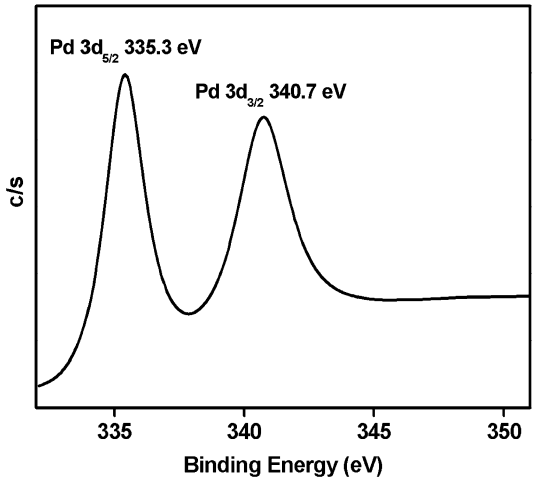

Fig. 2. XPS spectrum for Pd 3d regions of Pd–CNT composites prepared with the initial $PdCl_2$/CNTs weight ratio of 1:1.

to palladium oxides, which may be due to the slight oxidation of Pd nanoparticles upon exposure of the composites to ambient air.

The state of palladium deposited on CNTs can be further identified through XPS measurement. The XPS spectrum of Pd 3d regions of Pd–CNT composites is illustrated in Fig. 2, which reveals the presence of Pd $3d_{5/2}$ and $3d_{3/2}$ peaks at binding energy of 335.3 and 340.7 eV, respectively. Such binding energy values are in accordance with those reported for metallic Pd [30].

TEM is a powerful technique to get insight into the morphology and microstructure of the products. From TEM observation, it was found that about 60% CNTs were decorated with nanoparticles, and almost all nanoparticles deposited on the surfaces of CNTs in the view. Moreover, nanoparticles could not be separated from CNTs even after thorough washing and prolonged sonication. The strong adhesion between the nanoparticles and CNTs may result from the relatively high binding energy between Pd and CNTs [31]. From the images shown in Figs. 3a–3d, it can be observed that the surfaces of CNTs are decorated with nanoparticles of about 10 nm in diameter. Formation of the metallic Pd is further confirmed by the energy dispersive X-ray spectroscopy (EDS) analysis during the TEM observation (Fig. 3c). Element Cl, which will show two resolved peaks in the rectangular area, is not detectable in the EDS spectrum, indicating the conversion of $PdCl_2$ into Pd during the reaction process. As expected, the loading content of Pd nanoparticles onto the walls of CNTs increases with increasing the weight ratio of $PdCl_2$ to CNTs. Some nanoparticles even sinter together and subsequently form a nearly continuous and dense layer along the axis of CNTs at the $PdCl_2$/CNTs weight ratio of 2:1, as shown in Fig. 3d.

The high-resolution transmission electron microscopy (HRTEM) image of the products reveals the high crystallinity of the nanoparticles with visible lattices, as illustrated in Fig. 3e. Corresponding selected-area electron diffraction (SAED) pattern, given as an inset in Fig. 3b, presents typical Pd diffraction circles [32]. The diffraction does not exhibit as clear spots, but as concentric rings, each of which consists of a large number of very small spots, suggesting that the nanoparticles are composed of many fine crystallites. In addition to these circles, weak arcs from (002) reflection of hexagonal graphite structure can be observed as well.

For comparison, we performed reduction of $PdCl_2$ in liquid methanol with dispersed CNTs in the absence of SC CO_2 at 80 °C for 24 h. TEM observation for the sample shows that very few Pd particles are anchored onto CNTs, instead, free Pd aggregates with large size are yielded, as demonstrated in Fig. 3f. This control experiment confirms that SCF has some advantages in comparison with conventional liquid solvents for preparing the composites. With respect to liquids, the SCF possesses such properties as enhanced transport coefficient, gas-like viscosity and absence of surface tension, which promote the complete wetting of CNTs and are favorable to the adhesion of particles on the surfaces of CNTs. This result is similar to that reported by Wai and his co-workers, who deposited metallic Pd nanoparticles on CNTs via hydrogen reduction of corresponding organometallic compounds in SC CO_2 [20].

3.2. Synthesis of Ru–CNT nanocomposites

The similar procedures were applied to fabricate Ru–CNT nanocomposites using $RuCl_3 \cdot 3H_2O$ as a precursor in SC CO_2–methanol solution at 200 °C. The composites were characterized with different techniques.

Fig. 4 displays the XRD patterns of pristine CNTs and the as-prepared Ru–CNT composites. Besides the characteristic diffraction peaks of graphite, as shown in pattern (a), the additional peaks denoted in pattern (b) can be well assigned to the typical hexagonal phase of ruthenium [33]. The diffraction peaks at 42.2° and 44.0° appearing in pattern (b) can be attributed to the overlapping peaks corresponding to (100) and (101) reflections of graphite and (002) and (101) reflections of ruthenium. The XRD analysis indicates that ruthenium was formed in the process.

Fig. 5 shows the XPS spectrum for Ru 3p regions of the resulting Ru–CNT composites. The less intense Ru 3p signal was

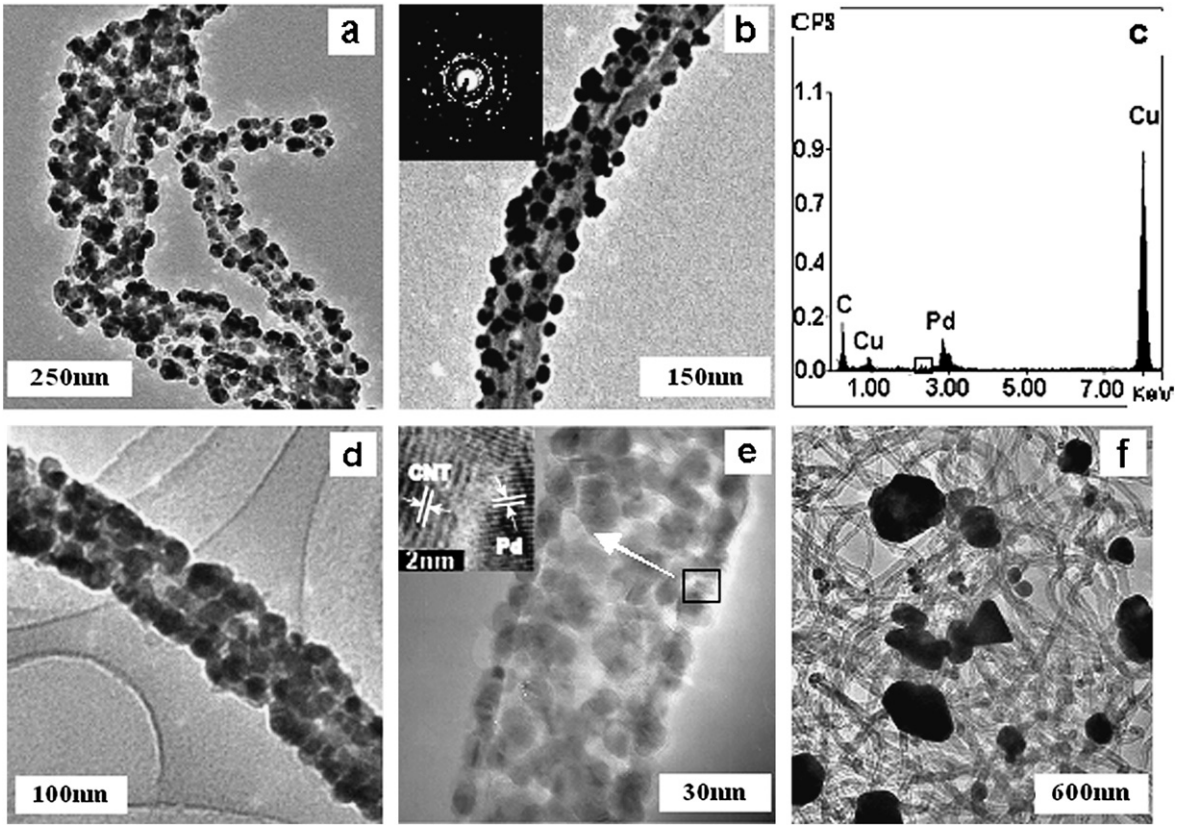

Fig. 3. TEM images of Pd–CNT composites: (a) low magnification and (b) high magnification, the inset is ED pattern of the composites. (c) EDS analysis of Pd–CNT composites. (d) High magnification TEM image of Pd–CNT composite. (e) HRTEM image of Pd–CNT composites. (f) TEM image of Pd–CNT composites synthesized via refluxing methanol solution at 80 °C. The initial $PdCl_2$/CNTs weight ratio for the composites shown in (a) and (d) is 1:1 and in (b), (c), (e) and (f) is 0.5:1.

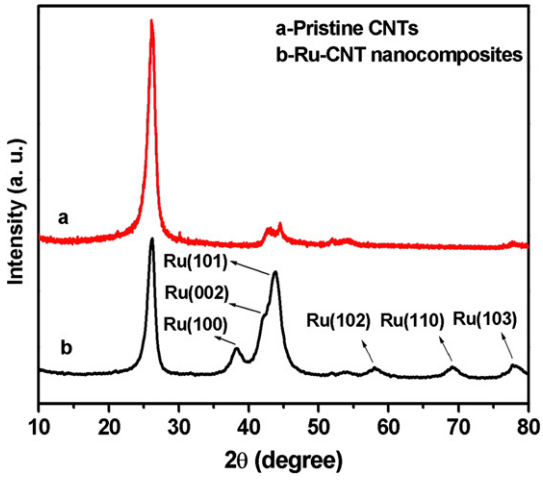

Fig. 4. XRD patterns of (a) pristine CNTs, (b) Ru–CNT composites prepared with the initial $RuCl_3 \cdot 3H_2O$/CNTs weight ratio of 1:1.

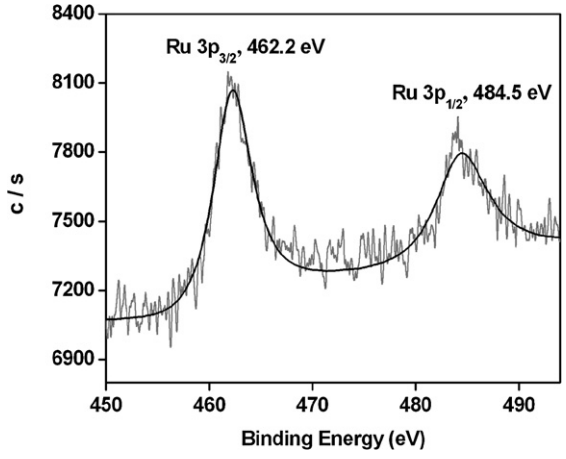

Fig. 5. XPS spectrum for Ru 3p regions of Ru–CNT composites synthesized with the initial $RuCl_3 \cdot 3H_2O$/CNTs weight ratio of 1:1.

analyzed instead of the main Ru 3d signal, as the latter is always obscured by C 1s signal. The spectrum presents a doublet, denoting two chemically different Ru entities with peak binding energy of Ru $3p_{1/2}$ at 484.5 eV and Ru $3p_{3/2}$ at 462.2 eV, which means that Ru(0) was formed through the reduction of $RuCl_3 \cdot 3H_2O$ in SC CO_2–methanol solution at 200 °C [34].

The morphology of the Ru–CNT nanocomposites was also examined by TEM. It was demonstrated that almost all nanoparticles were deposited on CNTs and almost all CNTs were decorated with nanoparticles. The mean size of Ru nanoparticles on CNTs is about 5 nm, estimated from TEM images displayed in Figs. 6a and 6b. The EDS result, as shown in Fig. 6c, illustrates the presence of ruthenium. Moreover, there is no peak of Cl in the EDS spectrum, which would appear in the rectangular area, implying the high purity of the composites. It is also observed that some Ru nanocrystals seem to insert into CNTs in the form of elongated particles, as depicted in Fig. 6d. The reason may

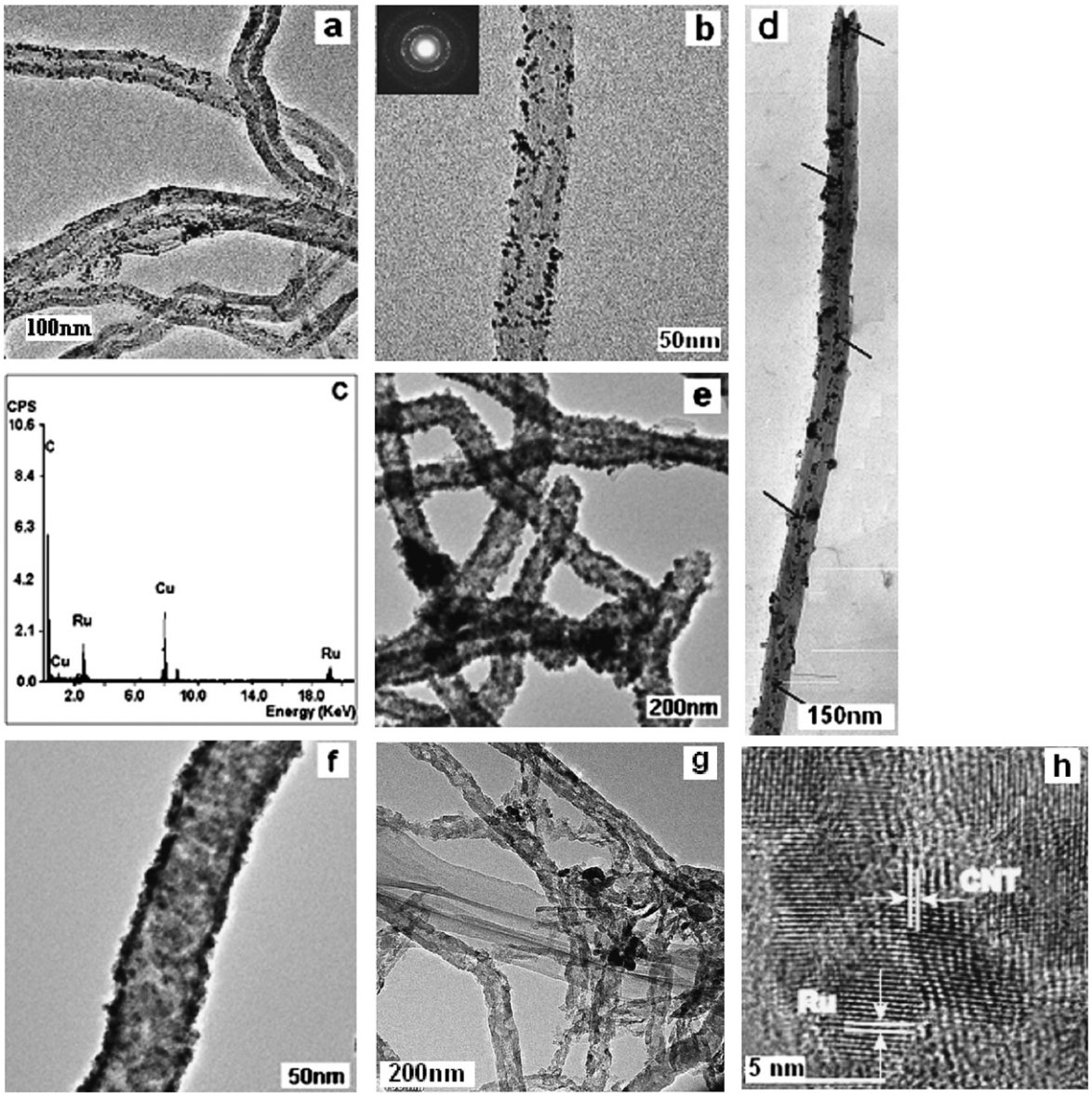

Fig. 6. (a) Low magnification TEM image of Ru–CNT composites. (b) High magnification TEM image of Ru–CNT composite, the inset is ED pattern of the composite. (c) EDS analysis of Ru–CNT composites. (d) TEM image of Ru–CNT composite filled with Ru particles. (e) Low magnification TEM image of Ru–CNT composites. (f) High magnification TEM image of Ru–CNT composite. (g) TEM image of the nanotubes and nanowires after the removal of CNTs, $RuCl_3{\cdot}3H_2O$/CNTs = 3:1. (h) HRTEM image of Ru–CNT composites. The initial $RuCl_3{\cdot}3H_2O$/CNTs weight ratio for the composites shown in (a)–(d), and (h) is 1:1 and in (e) and (f) is 3:1.

be that some $RuCl_3$ dissolved in SC CO_2–methanol solution can diffuse into the interior of CNTs and form Ru nanoparticles in the CNT cavities via reaction between $RuCl_3$ and methanol. Similarly, the loading content of Ru nanocrystals on CNTs can be tuned by controlling the relative mass ratio of $RuCl_3{\cdot}3H_2O$ to CNTs. As can be clearly seen from Figs. 6e and 6f, CNTs are even fully wrapped with continuous Ru nanoparticle layers when the initial mass ratio of $RuCl_3{\cdot}3H_2O$/CNTs increases to be 3:1. Moreover, on heating the Ru-coated CNTs at 500 °C for 6 h, the nanotubes were oxidized, yielding the RuO_2 (verified by XRD analysis, not shown here) nanostructures shown in the TEM image in Fig. 6g.

HRTEM inspection (Fig. 6h) demonstrates the crystalline quality of Ru nanoparticles with distinct lattice fringes. SAED pattern given as an inset in Fig. 6b shows characteristic Ru diffraction rings, which also confirms the crystalline nature of Ru nanoparticles in the composites [35].

3.3. Possible formation mechanism of the composites

The formation mechanism of the metallic nanocrystal–CNT nanocomposites through an inorganic reaction route can be discussed as follows. It was reported that $PdCl_2$ [36,37] and $RuCl_3$ [38] could react with methanol, and the reactions can be expressed by the following equations:

$$PdCl_2 + CH_3OH \rightarrow Pd + HCHO + 2HCl,$$

$$2RuCl_3 + 3CH_3OH \rightarrow 2Ru + 3HCHO + 6HCl.$$

We believe that the reactions in SC CO_2–methanol solution of this work are the same as above due to the inert nature of CO_2. This was confirmed by the fact that HCHO was detected in the extracted byproducts by gas chromatography analysis. Our experiments showed that the two inorganic precursors were not soluble in SC CO_2, but were soluble in SC CO_2–methanol solution at our experimental conditions. Therefore, it can be deduced that methanol served as reductant as well as cosolvent for enhancing the dissolubility of $PdCl_2$ and $RuCl_3$ in the SC CO_2-based solutions. The zero surface tension of SC CO_2–methanol fluid facilitated complete wetting of CNTs with the precursor solutions. As the reaction proceeded, the produced metal atoms aggregated to form nanoparticles, preferably depositing on the surfaces of CNTs. The produced HCHO and HCl dissolved in SC CO_2–methanol solution could be easily removed via extraction with SC CO_2 after reaction. As a consequence, dry metal-decorated CNT nanocomposites were obtained.

TEM examination showed that some Ru nanocrystals were incorporated into the interior of CNTs, while no Pd nanoparticle was filled into CNTs. This may be resulted from the different reaction rate of $PdCl_2$ and $RuCl_3$ with methanol. Under our experimental conditions, $RuCl_3$ dissolved in SC CO_2–methanol solution could diffuse into the inner cavities of CNTs prior to reaction with methanol, and subsequently form Ru nanoparticles in CNTs at reaction temperature. However, $PdCl_2$ dissolved in SC CO_2–methanol solution was probably reduced readily by methanol before being transferred into CNTs, therefore, the produced Pd nanoparticles preferably deposited on the outer surfaces of CNTs.

4. Conclusions

Pd–CNT and Ru–CNT nanocomposites have been fabricated through reduction reactions of $PdCl_2$ and $RuCl_3{\cdot}3H_2O$ in SC CO_2–methanol solutions in the presence of CNTs, respectively. In this route, methanol serves as reductant for the metal precursors as well as cosolvent to enhance the solubility of the precursors in SC CO_2. At suitable conditions, Pd and Ru nanocrystals produced are firmly anchored to CNTs. The loading content and particle size of the nanoparticles can be tuned by manipulating the mass ratio of the precursor to CNTs. We believe that this convenient and effective approach may be potentially extended to prepare other metal–CNT composites.

Acknowledgments

This work is financially supported by National Natural Science Foundation of China (No. 50472096) and opening research fund of state key laboratory of heavy oil processing (No. 2004-10).

References

[1] H.J. Dai, J.H. Hafner, A.G. Rinzler, D.T. Colbert, R.E. Smalley, Nature 384 (1996) 147.
[2] W.A. De-Heer, A.D. Cha-Telain Ugarte, Science 270 (1995) 1179.
[3] J. Kong, N.R. Franklin, C. Zhou, M.G. Chapline, S. Peng, K. Cho, H. Dai, Science 287 (2000) 622.
[4] C. Liu, Y.Y. Fan, M. Liu, H.T. Cong, H.M. Cheng, M.S. Dresselhaus, Science 286 (1999) 1127.
[5] M. Burghard, K. Balasubramanian, Small 1 (2005) 180.
[6] J. Chen, H. Liu, W.A. Weimer, M.D. Halls, D.H. Waldeck, G.C. Walker, J. Am. Chem. Soc. 124 (2002) 9034.
[7] J. Kong, M.G. Chapline, H. Dai, Adv. Mater. 13 (2001) 1384.
[8] S.G. Wang, Q. Zhang, R. Wang, S.F. Yoon, J. Ahn, D.J. Yang, J.Z. Tian, J.Q. Li, Q. Zhou, Electrochem. Commun. 5 (2003) 800.
[9] J.M. Planeix, N. Coustel, B. Coq, V. Brotons, P.S. Kumbhar, R. Dutartre, P. Geneste, P. Bernier, P.M. Ajayan, J. Am. Chem. Soc. 116 (1994) 7935.
[10] G. Che, B.B. Lakshmi, E.R. Fisher, C.R. Martin, Nature 393 (1998) 346.
[11] Y. Lin, X. Cui, C.H. Yen, C.M. Wai, Langmuir 21 (2005) 11474.
[12] Y. Lin, X. Cui, C.H. Yen, C.M. Wai, J. Phys. Chem. B 109 (2005) 14410.
[13] Z.Y. Sun, Z.M. Liu, B.X. Han, Y. Wang, J.M. Du, Z.L. Xie, G.J. Han, Adv. Mater. 17 (2005) 928.
[14] B. Yoon, C.M. Wai, J. Am. Chem. Soc. 127 (2005) 17174.
[15] J.A. Darr, M. Poliakoff, Chem. Rev. 99 (1999) 495.
[16] J.F. Bocquet, K. Chhor, C. Pommier, Surf. Coat. Technol. 70 (1994) 73.
[17] F. Cansell, B. Chevalier, A. Demourgues, J. Etourneau, C. Even, Y. Garrabos, V. Pessey, S. Petit, A. Tressaud, F. Weill, J. Mater. Chem. 9 (1999) 67.
[18] H. Wakayama, N. Setoyama, Y. Fukushima, Adv. Mater. 15 (2003) 742.
[19] J.M. Blackburn, D.P. Long, A. Cabanas, J.J. Watkins, Science 294 (2001) 141.
[20] X.R. Ye, Y.H. Lin, C.M. Wang, C.M. Wai, Adv. Mater. 15 (2003) 316.
[21] J. Qian, M.T. Timko, A.J. Allen, C.J. Russell, B. Winnik, B. Buckley, J.I. Steinfeld, J.W. Tester, J. Am. Chem. Soc. 126 (2004) 5465.
[22] M.J. Burk, S. Feng, M.F. Gross, W. Tumas, J. Am. Chem. Soc. 117 (1995) 8277.
[23] D. Koch, W. Leitner, J. Am. Chem. Soc. 120 (1998) 13398.
[24] M. Kondo, K. Rezaei, F. Temelli, M. Goto, Ind. Eng. Chem. Res. 41 (2002) 5770.
[25] M.T. Reetz, W. Wiesenhöfer, G. Franciò, W. Leitner, Adv. Synth. Catal. 345 (2003) 1221.
[26] A. Tavana, J. Chang, A.D. Randolph, N. Rodriguez, AIChE J. 35 (1989) 645.
[27] Q. Liang, B.C. Liu, S.H. Tang, Z.J. Li, Q. Li, L.Z. Gao, B.L. Zhang, Z.L. Yu, Acta Chim. Sin. (Chin. Ed.) 58 (2000) 1336.
[28] A. Cao, C. Xu, J. Liang, D. Wu, B. Wei, Chem. Phys. Lett. 344 (2001) 13.
[29] A. Fukuoka, H. Araki, Y. Sakamoto, S. Inagaki, Y. Fukushima, M. Ichikawa, Inorg. Chim. Acta 350 (2003) 371.
[30] D. Bera, S.C. Kuiry, M. McCutchen, A. Kruize, H. Heinrich, M. Meyyappan, S. Seal, Chem. Phys. Lett. 386 (2004) 364.
[31] S. Ciraci, S. Dag, T. Yildirim, O. Gülseren, R.T. Senger, J. Phys. Condens. Matter 16 (2004) R901.
[32] Y. Hayashi, T. Tokunaga, S. Toh, W.J. Moon, K. Kaneko, Diam. Relat. Mater. 14 (2005) 790.
[33] J. Chen, Z.L. Tao, S.L. Li, J. Am. Chem. Soc. 126 (2004) 3060.
[34] C. Bock, C. Paquet, M. Couillard, G.A. Botton, B.R. MacDougall, J. Am. Chem. Soc. 126 (2004) 8029.
[35] M.C. Lafont, F. Juarez, L.C. Vahlas, Scripta Mater. 51 (2004) 699.
[36] S. Horiuchi, T. Fujita, Langmuir 19 (2003) 2963.
[37] T. Hashimoto, M. Harada, N. Sakamoto, Macromolecules 32 (1999) 6867.
[38] X. Wang, I.M. Hsing, Electrochim. Acta 47 (2002) 2981.